Research Article Vol. 12, No. 4 / 1 Apr 2022 / Optical Materials Express 1323
Optical Materials EXPRESS

Tunable distributed sensing performance in Ca-based nanoparticle-doped optical fibers

VICTOR FUERTES,* NICOLAS GRÉGOIRE, STEEVE MORENCY, STÉPHANE GAGNON, YANNICK LEDEMI, SOPHIE LAROCHELLE, AND YOUNÈS MESSADDEQ

Centre d'optique, Photonique et Laser, 2375 Rue de la Terrasse, Université Laval, Québec, (QC), G1 V 0A6, Canada
victor.fuertes-de-la-llave.1@ulaval.ca

Abstract: Rayleigh scattering enhanced nanoparticle-doped optical fibers is a technology very promising for distributed sensing applications, however, it remains largely unexplored. This work demonstrates for the first time the possibility of tuning Rayleigh scattering and optical losses in Ca-based nanoparticle-doped silica optical fibers by controlling the kinetics of the re-nucleation process that nanoparticles undergo during fiber drawing by controlling preform feed, drawing speed and temperature. A 3D study by SEM, FIB-SEM and optical backscatter reflectometry (OBR) reveals an early-time kinetics at 1870 °C, with tunable Rayleigh scattering enhancement 43.2–47.4 dB, regarding a long-haul single mode fiber, SMF-28, and associated sensing lengths of 3–5.5 m. At 2065 °C, kinetics is slower and nanoparticle dissolution is favored. Consequently, enhanced scattering values of 24.9–26.9 dB/m and sensing lengths of 135–250 m are attained. Finally, thermal stability above 500 °C and tunable distributed temperature sensitivity are proved, from 18.6 pm/°C to 23.9 pm/°C, ~1.9–2.4 times larger than in a SMF-28. These results show the promising future of Rayleigh scattering enhanced nanoparticle-doped optical fibers for distributed sensing.

1. Introduction

Nanoparticle-doped silica-based optical fiber is a field that is receiving great interest in recent years due to the promising technological opportunities it offers for a broad range of applications such as sensors, high-power fiber lasers, fiber amplifiers, etc [1,2]. The presence of nanoparticles in the silica-based matrix allow incorporating new functionalities while maintaining the favorable properties that silica glass presents [1,3]. Different types of nanoparticles have been considered in literature, such as metallic, semiconductor or ceramic ones, which along with their physical features are intimately linked with the functionality that is intended to be incorporated [4,5]. Nevertheless, the presence of nanoparticles might constrain their applicability, because of the increase in optical attenuation associated with the rise in Rayleigh scattering induced by the presence of nanoparticles. This type of scattering is caused when the light is dispersed by particles of size much smaller than the light wavelength. However, this drawback has been recently used to fabricate distributed optical fiber sensors (DOFS) based on Rayleigh scattering enhancement [6,7]. DOFS are of particular interest, since they allow the sensing of multiple physical and chemical parameters such as strain, stress, temperature, magnetic field, radiation, gas or refractive index, among others, with spatial resolution along the entire fiber [8–10]. In particular, through the detection of Rayleigh backscattering in frequency domain by optical backscatter reflectometry (OBR), a high spatial resolution up to ten microns over ten-meter-level range can be achieved [11]. From the analysis of spectral shifts in the Rayleigh backscattering spectra, changes of strain or temperature, for instance, can be measured and its sensitivity calibrated [12]. So far, the suitability of Rayleigh scattering enhanced nanoparticle-doped optical

#451311 https://doi.org/10.1364/OME.451311
Journal © 2022 Received 13 Dec 2021; revised 18 Feb 2022; accepted 21 Feb 2022; published 4 Mar 2022

Optical Materials EXPRESS

fibers has been demonstrated for only some few compositions: MgO- and CaO- based amorphous nanoparticles grown *in situ* in the core of preforms during the fabrication process [6,7,13].

This approach based on phase separation of alkaline-earth nanoparticles in a silica-based matrix during the preform fabrication process has shown a high performance in terms of a good trade-off between Rayleigh scattering increase, with respect to a SMF-28 fiber, and two-way attenuation. Values up to 48.9 dB and 14.3 dB/m, respectively, for MgO nanoparticles doped optical fibers have been reported [14] and recently, tunable enhanced backscattering in the range 25.9–44.9 dB, paired with low two-way optical losses, 0.1–8.7 dB/m, for CaO nanoparticles doped optical fibers [7]. Regarding this last work, we demonstrated that the Ca-based nanoparticles presented in the preform core undergo a dissolution phenomenon during fiber drawing process and re-nucleation afterwards as a function of drawing temperature. Consequently, Ca-based nanoparticles can be tailored in shape, size and density, in a wide temperature range, which allow reaching long-range sensing lengths, from 5 m to more than 200 m. Thus, this work has opened a new venue for this type of nanoparticle-doped optical fibers, since drawing conditions might be adjusted, taking into consideration the kinetic of the re-nucleation of nanoparticles in the glass system, to fit the desired final characteristic of the targeted DOFS. However, this issue has not been considered in literature, so far, and not only in the field of distributed sensing but also in the whole field of nanoparticle-doped optical fibers.

The possibility of distributed sensing parameters such as temperature [6,14], 3D shape sensing [15], strain [6,14] and refractive index [16–18] have been demonstrated in MgO nanoparticles doped optical fibers by Blanc et al. which has increased the research interest of this new technology for future potential applications. However, despite of the recent progress in the field, the doping of the core of silica-based fibers with nanoparticles for distributed sensing applications is still in an initial phase and more research studies are required, primarily from a material science point of view, in order to understand how the fabrication process might impact on the nanoparticle features and therefore maximizing the performance of the DOFS.

In this context, the aim of this work is to deepen the knowledge about these novel Ca-based nanoparticle-doped silica-based optical fibers and study how the kinetics of the system determine the re-nucleation phenomena of nanoparticle during fiber drawing, and thus their characteristics and the induced Rayleigh scattering. For that purpose, different preform feed, drawing speed and drawing temperatures are considered during fiber fabrication. Their impact on the Ca-based nanoparticles, the enhancement of Rayleigh scattering and the associated optical losses, is assessed by a thorough study with Scanning electron microscopy (SEM), Focused Ion Beam-SEM (FIB-SEM) and OBR. Finally, in order to investigate their applicability as DOFS, in particular for temperature sensing, their thermal sensitivity is experimentally extracted by OBR while heating the fiber samples at temperatures in the range 30–120 °C. The thermal stability for potential high-temperature applications is also evaluated.

2. Materials and methods

2.1. Preform and fiber fabrication

A silica-based preform doped with Ca-based nanoparticles was fabricated by the conventional MCVD method along with a solution doping technique. The porous silica layer was soaked with a solution of 5 mM of $CaCl_2$ in water and vitrified at 1800 °C, while the preform collapse was above 2000 °C. $CaCl_2$ is soluble in water which favor a homogeneous impregnation of the soot. This low concentration is necessary to target fibers that combine relatively low optical losses with considerable values of enhanced Rayleigh scattering [7]. The diameter of the preforms was ~15 mm and the core diameter of ~1.2 mm. Further details about the preform fabrication process can be found in Fuertes et al. [7]. GeO_2 and P_2O_5 are introduced in gas phase during the preform fabrication in order to enhance the refractive index of the core with respect to the cladding and create a refractive index difference (Δn), of $\sim 10 \times 10^{-3}$ (Fig. 1(a)). About 6 mol.% GeO_2 and 1

Optical Materials EXPRESS

mol.% P_2O_5 were presented in the preform core. Based on previous works [7], both the GeO_2 and P_2O_5 content as well as the nanoparticle concentration in the preform core contribute to the measured Δn. Ca-rich nanoparticles are grown *in situ* in the core of the preform by employing the spontaneous phase separation that alkaline-earth elements undergo in silicate systems in the range of temperatures reached during the preform fabrication process [7,19].

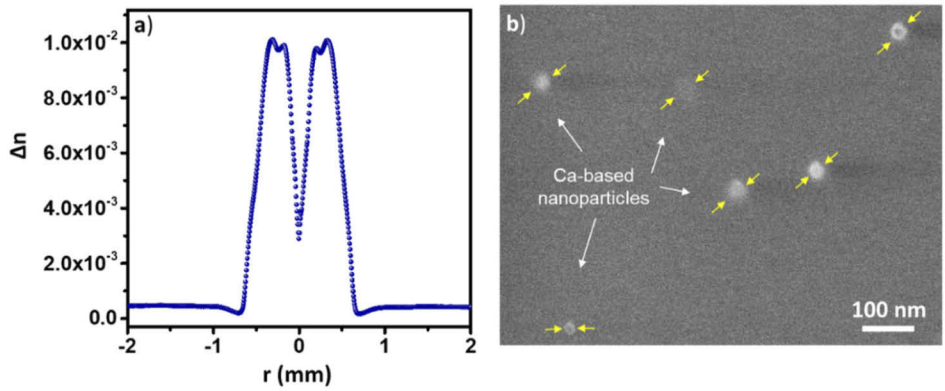

Fig. 1. Characterization of the Ca-based nanoparticle-doped preform. **a)** Refractive index profile. **b)** SEM micrograph of the core that shows characteristic Ca-based nanoparticles, marked with yellow arrows.

Figure 1(b) shows a representative SEM micrograph of the preform core, in which characteristic Ca-based nanoparticles are observed. Some nanoparticles appear as blurry spots since they are located under the surface analyzed. The nanoparticles, display sizes generally below 100 nm, with a mean diameter of ~50 nm and totally dispersed in the preform core, with an inter-particle distance generally of hundreds of nanometers up to several microns [7]. All these features have been demonstrated to be key for attaining low-loss nanoparticle-doped optical fibers [7]. The composition of the nanoparticles grown *in situ*, based on previous works [7], is Ca-enriched (40–45 mol.%), and composed of phosphorus, ~11 mol.%, germanium, ~3–4 mol.%, of the corresponding oxides as well as SiO_2 (40–46 mol.%). The optical fibers are drawn from the fabricated preform on a drawing tower at two different temperatures, 1870 °C and 2065 °C, with a variable preform feed and drawing speed according to Table 1. Fiber A and D were drawn from the initial preform of ~15 mm in diameter. However, for the drawing of Fiber B,C as well as E,F the preform was stretched to a diameter of ~8 mm, in order to vary the feed and drawing speed, according to Table 1, while maintaining the same fiber dimensions. All fibers were designed to match with SMF-28 telecom fibers and have an external diameter of 125 μm and a core diameter of ~10 μm, which permits their manipulation as in standard ones. These drawing temperatures are selected because we demonstrated that the corresponding Ca-based nanoparticle-doped optical fibers display a trade-off between Rayleigh backscattering enhancement and optical losses suitable for different long-range sensing lengths, ranging from ~5 m to more than 200 m, respectively [7].

2.2. Microstructural characterization

Microstructural characterization of the preform and fibers was carried out by means of a FEI QUANTA 3D FEG Scanning Electron Microscope, with a resolution of 1.5 nm at 30 kV in Secondary Electron (SE) and low vacuum mode. Focused ion beam (FIB) along with SEM were used to investigate the nanoparticle features in three dimensions. The volume was etched by using a 30 kV and 3 nA of Ga ion beam. SEM micrographs in the FIB-SEM mode were obtained by tilting the fiber sample at 50° angle between the fiber surface and the ion beam incidence

Optical Materials EXPRESS

Table 1. Summary of the different Ca-based nanoparticles doped fiber drawing conditions for the samples A-F studied in this work.

Fiber designation	Drawing temperature (°C)	Preform feed (mm/min)	Drawing speed (m/min)	Tension (g)
A	1870	0.3	5	119
B	1870	1.3	5	121
C	1870	2	8	138
D	2065	0.4	8	35
E	2065	3.1	12	52
F	2065	4.9	20	78

direction. Particle size along the z-axis was measured taking into consideration the tilt correction. Dimensions of the analyzed area after etching process were around $6 \times 1 \times 12$ µm.

2.3. Optical characterization

Refractive index profile of the fabricated preforms was measured by using a Photon Kinetics PK2600 Preform Analyzer. OBR measurements of the enhanced backscattering fibers were carried out by using a commercial Luna OBR 4600, characterized by a sensitivity of −130 dB and a spatial resolution of 20 µm. For the measurements, the different nanoparticle-doped fibers were spliced to a SMF-28 fiber pigtail ending in a FC/APC connector and connected to the OBR 4600. The fibers were evaluated with a laser input centered at 1550 nm and a wavelength range of 43 nm, sweeping in the telecommunication window and taking 16,384 sensing points per analysis. For time-domain measurements, the Fourier analysis of the backscattered signal, made by the software, allow obtaining the Rayleigh backscattered intensity along the fiber length. Temperature effect is evaluated in frequency-domain. Wavelength shift caused by temperature of selected fibers is monitored by the Luna OBR 4600, with a resolution bandwidth of 2 GHz. From the slope extracted from the linear fitting of the wavelength shift vs temperature, the temperature sensitivity is obtained.

3. Results and discussion

3.1. Influence of drawing conditions on Ca-based nanoparticle features in-plane and along drawing direction: SEM and FIB-SEM characterization

With the aim of investigating the effect of factors such as time and temperature on the re-nucleation phenomena of nanoparticles during the fiber drawing process, and therefore their characteristics, SEM measurements from the fiber samples A-F were carried out. As it was established in previous works [7], the number density of particles for this type of fibers, that is, drawn from preforms made from solutions of 5 mM of $CaCl_2$ is generally very low, and it considerably decreases as drawing temperature increases due to the dissolution of the nanoparticles. Figure 2 shows representative cross-section SEM micrographs of fibers A (Fig. 2(a)), fiber B (Fig. 2(b)) and fiber C (Fig. 2(c)), in which the characteristic morphology and size can be observed. Moreover, the corresponding histograms elaborated after analyzing eight representative surfaces for each fiber sample are depicted in Fig. 2(d)-(f), respectively, and allow extracting some information about the kinetics of the system. It is worth pointing out that the boundary between a nanoparticle and the glass is usually blurry, then all the measured sizes have an estimated error of ~5 nm. Fiber A displays a behavior similar to the one reported in [7], being mainly characterized by elongated particles of more than 200 nm (right-bottom inset of Fig. 2(a)), and some spherical nanoparticles (right-top inset of Fig. 2(a)), to a lesser extent, with diameters ranging from ~20 nm to 154 nm (Fig. 2(d)). However, as drawing time decreases, both by increasing preform feed and drawing speed (see Table 1), while maintaining the drawing temperature constant at 1870 °C, spherical

Optical Materials EXPRESS

nanoparticle number density considerably rises, with a mean diameter size that also tends to increase and is predominant instead of elongated ones. Thus, since the spherical nanoparticles are the ones more common between fiber A-C, the study presented in the histograms depicted in Fig. 2(d)-(f) is focused on the spherical nanoparticles. In particular, fiber C shows nanoparticles up to 233 nm and a mean diameter size of 118 nm, while fiber A shows no spherical nanoparticle longer than 154 nm and about 97 nm on average. Fiber B displays approximately the same mean diameter size as fiber C but the dispersion is lower, with a maximum nanoparticle size measured of 198 nm. This implies an increase of XY particle size ~20% regarding fiber A. With respect to inter-particle distance, overall, as nanoparticle number density increases, the inter-particle distance tends to decrease, being the closest nanoparticles ~500 nm, from each other, in fibers A and ~100 nm in the fibers B and C. As it was previously stated, the nanoparticles present in the preform have a mean diameter size of ~50 nm, nevertheless, the average diameter size of the nanoparticles in the fibers increase up to 97–118 nm, for fibers A-C, depending on the drawing conditions. In previous works [7], it was suggested that the Ca-based nanoparticles presented in the core of the preform are dissolved during the drawing process, and a re-nucleation follows, as a temperature dependent process, according to the phase diagram of SiO_2-CaO [20]. Based on the above discussion, this phenomenon is confirmed, being both time-dependent and temperature-dependent. At 1870 °C, in terms of nanoparticle number density, diameter size and inter-particle distance no remarkable differences are observed between fiber B and fiber C, while in fiber A these parameters are considerably affected, which suggest an early-time kinetics of these Ca-based nanoparticles, while at longer-times dissolution phenomena starts to play an important role, decreasing nanoparticle number density and size. Moreover, the elongated shapes observed, mainly in fiber A, seem to be strongly dependent on the drawing time and consequently on the kinetics of the re-nucleation process, appearing mainly for lower preform feeds and drawing speeds while disappearing for higher ones. Regarding the location of nanoparticles, they are usually randomly distributed around the fiber core in all fibers, independently of drawing conditions, and there is a tendency of the nanoparticles to re-nucleate in the surroundings, close from each other as it can be seen in Fig. 2(a)-(c).

To further examine these fibers in their volume and extend the influence of the fiber drawing variables previously discussed on the spherical nanoparticles contained in the fiber core, a FIB-SEM analysis of optical fibers A-C was carried out, and the corresponding micrographs are depicted in Fig. 3.

In the fiber volume, a similar trend as for the in-plane analysis is observed, that is, an increase of particle size and number density along with a decrease of inter-particle distance as drawing time decreases, from fiber A to fiber C. Fiber A shows nanoparticles with a Z size in the range 180–185 nm (Fig. 3(a)), while fibers B-C in the range 195–245 nm and 186–290 nm (Fig. 3(b),(c)), respectively. The average Z size of these nanoparticles observed in Fig. 3 are ~ 183 nm for fiber A and ~ 225 nm for fibers B-C, which supposes an increase of ~ 40–44% with respect to the average particle size measured for the x axis (Fig. 3). Particle size along the z-axis was measured taking into consideration the tilt correction. These results agree with the previous discussion for the cross-section observations, and it can be stated that at 1870 °C, regarding nanoparticle size, no remarkable differences are observed between fiber B and fiber C, while nanoparticles in fiber A are considerably lower, apart from having a lower number density. These findings support the previous suggestion about the presence of early-time kinetics of the re-nucleation of Ca-based nanoparticles in the glass system.

Based on the morphology of the particles observed in the volume, Fig. 3, it might be assumed that correspond to the nanoparticles observed as spherical in the xy-plane. Then, the nanoparticles observed as spherical in the xy-plane tend to be elongated along the drawing direction, because of the drawing process. The size of the largest particles in z-direction regarding the largest ones observed in the xy-plane is up to 20% for fiber A and ~24% for fibers B and C. It is important to

Optical Materials EXPRESS

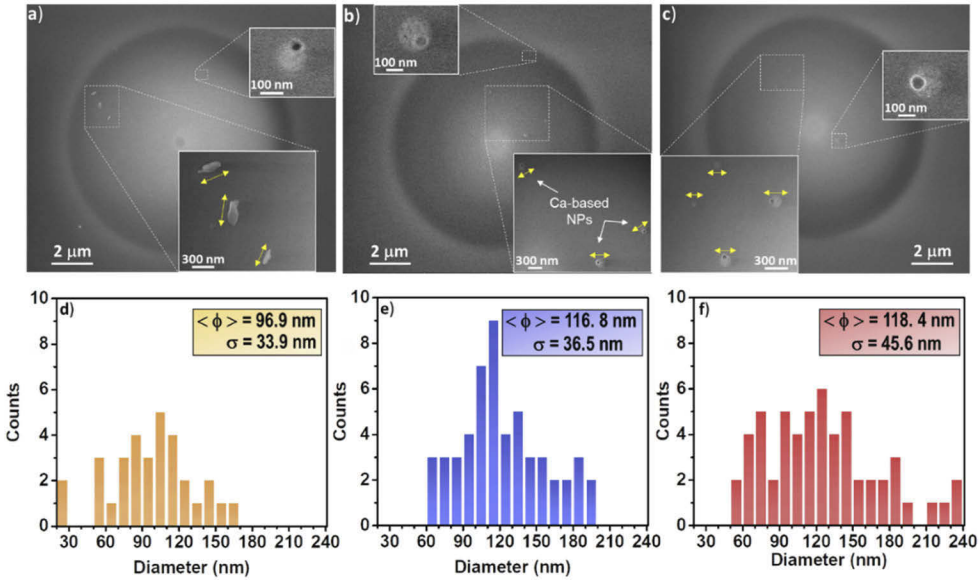

Fig. 2. Representative cross-section SEM micrographs of: **a)** fiber A; **b)** fiber B and **c)** fiber C. The insets show in more detail the characteristic morphology and size of particles for the corresponding fiber. Some holes appear on nanoparticle surface after electron beam irradiation. Histograms depict the number of spherical-shaped nanoparticles, and the particle distribution size for: **d)** fiber A; **e)** fiber B and **f)** fiber C. The mean diameter (<Ø>) and standard deviation (σ) is included as inset for every fiber. Elongated particles are not considered for the histograms. The uncertainty for each nanoparticle measurement is estimated ~5 nm. The abbreviation NPs = nanoparticles are used.

point out that although the decrease of drawing time allows increasing the nanoparticle number density, that remains still very low for the different fibers, with less than six nanometric particles in a scanned area of ~12 µm in depth (Fig. 3(c)). This low concentration of nanoparticles is a requirement to minimize optical losses associated with Rayleigh scattering. Further studies will be necessary to analyze in detail how is the shape of the elongated particles observed in the xy-plane along the fiber volume.

Optical fibers D-F, drawn at 2065 °C, show much lower nanoparticle number density and size, as a consequence of their dissolution in the silica-based glass during the drawing process, with one or two Ca-based nanoparticles per analyzed cross-section surface (Fig. 4), in agreement with [7]. This very low number density hampers an in-depth study, like the one carried out for fibers A-C. In general, fibers D-F display more similar nanoparticles features, which suggests a slower kinetics at higher drawing temperatures, showing high sphericity and sizes ranging from ~ 20 nm to 90 nm, independently of drawing conditions (Fig. 4). Dissolution phenomena should be lessened from fibers F to D, because of the decrease of drawing time. Although it is difficult to appreciate it by SEM, probably due to more subtle differences, the enhancement of Rayleigh scattering should decrease from fibers F to D, based on the above explanation, as it will be discussed further in the next section.

These findings demonstrate the possibility of tailoring nanoparticle characteristics by means of drawing conditions, such as drawing speed, preform feed, for the first time, and drawing temperature. Although the kinetics of the system is mainly determined by temperature, time might also play an important role in the nanoparticle characteristics, especially at low drawing temperatures. In terms of tension, according to Table 1, the higher the tension, the higher the

Optical Materials EXPRESS

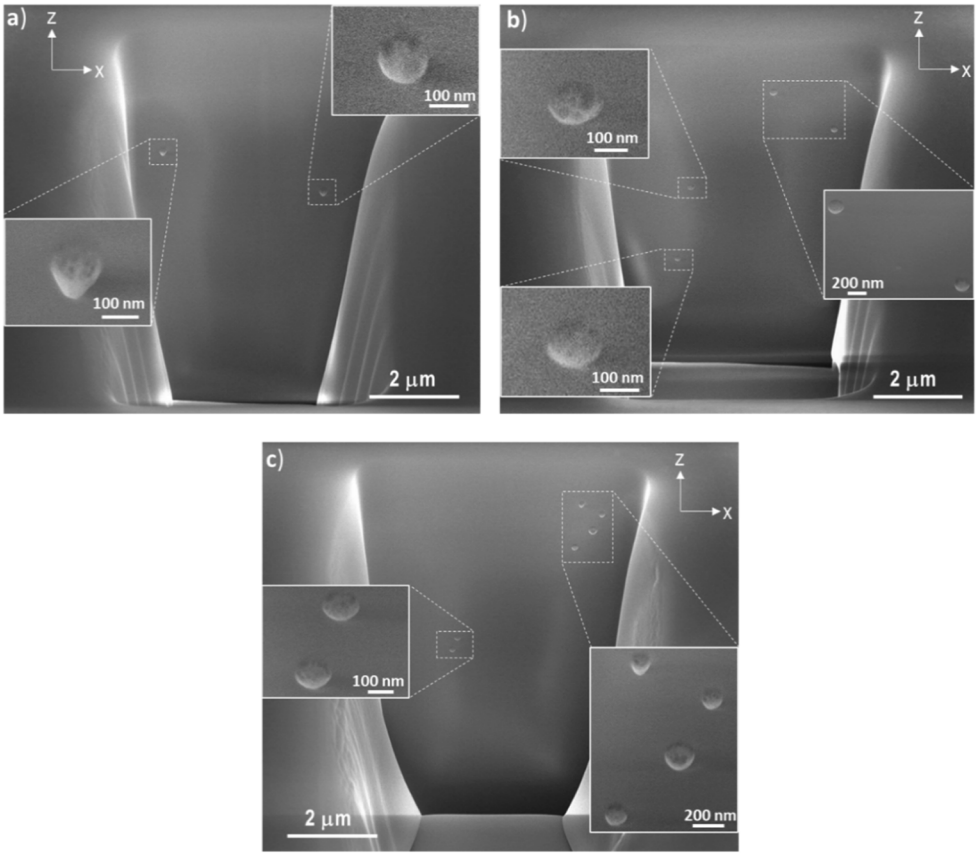

Fig. 3. FIB-SEM micrographs of longitudinal sections from the optical fiber core obtained by tilting the fiber sample at 50° angle between the fiber surface and the ion beam incidence direction, for **a)** fiber A; **b)** fiber B; **c)** fiber C. Insets show in more detail the influence of the different drawing conditions on the nanoparticle characteristics along the drawing direction. Particle size along the z-axis was measured taking into consideration the tilt correction. Nanoparticles increase their average size along drawing direction ~ 40% for fiber A and ~ 44% for fibers B-C, with respect to the average particle size measured for the x axis.

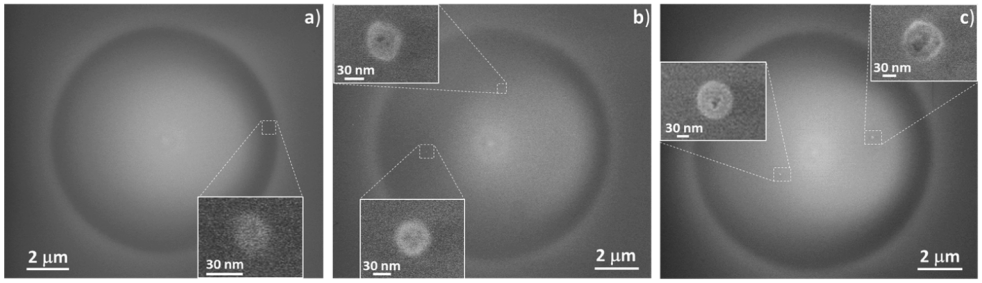

Fig. 4. Representative cross-section SEM micrographs of: **a)** fiber D; **b)** fiber E and **c)** fiber F. The insets show in more detail the characteristic morphology and size of particles for the corresponding fiber. Some holes appear on nanoparticle surface after electron beam irradiation.

Optical Materials EXPRESS

nanoparticle size and number density, and consequently lower the inter-particle distance. All these factors will have a direct impact on the Rayleigh scattering of light, as it will be discussed in next section, due to the high dependence on factors such as nanoparticle size, number density or inter-particle distance, among others.

3.2. Tuning of Rayleigh scattering enhancement by drawing conditions: optical backscatter reflectometry measurements

Figure 5 depicts the enhancement of Rayleigh backscattered intensity measured along the fiber length by OBR for the Ca-based nanoparticles doped optical fibers A-F. All fibers are spliced with an SMF-28 fiber, therefore, the enhanced backscattering intensity, marked with a red arrow in each plot of Fig. 5, is relative to the SMF-28 fiber considered as reference. With respect to the optical attenuation (considering forward and backward scattering), caused by the presence of the Ca-based nanoparticles in the fiber core, is estimated by a linear regression of the slope of the curve, marked by a red line. At drawing temperature 1870 °C, fibers A-C show considerable dependence on drawing time as it was also previously stated for the corresponding nanoparticle features, in section 3.1. Consequently, the enhancement of Rayleigh backscattering might be tuned in the range 43.2–47.4 dB, and it is paired with two-way optical losses of 8.0–14.6 dB/m. The effect of increasing preform feed from 0.3 mm/min to 1.3 mm/min while maintaining drawing speed at 5 m/min, respectively for fibers A and B, is to increase 3.4 dB the intensity signal and 3.9 dB/m the optical attenuation. This is explained due to the presence of larger nanoparticle density and with larger size in fiber B regarding fiber A, according to the conclusions extracted from SEM and FIB-SEM measurements in section 3.1, which increases the scattering of light and therefore the optical losses (according to eq. (S.1) and (S.2) of Supporting information S1). Fiber C increases these values an extra 0.8 dB and 2.7 dB/m, respectively, regarding fiber B, as a consequence of the rise in preform feed and drawing speed to 2 mm/min and 8 m/min, reaching values up to 47.4 dB and 14.6 dB/m. As a result, the sensing length might be varied between 3 m and 5.5 m in fibers A-C, while maintaining a good trade-off between Rayleigh backscattering and optical attenuation. OBR measurements confirm an early-time kinetics in the re-nucleation process that the Ca-based nanoparticles undergo during the fiber drawing at lower drawing temperatures, as it was previously suggested in section 3.1, with more subtle differences between fibers B and C while remarkable ones between fiber A and fibers B,C.

At a higher drawing temperature, 2065 °C, fibers D-F also show dependence on drawing conditions, although to a lesser extent than fibers A-C, as it was anticipated by SEM measurements. In this case, to increase preform feed 2.7 mm/min and drawing speed 4 m/min, from preform D to preform E, only increases the Rayleigh backscattering intensity 0.5 dB while optical attenuation remains approximately the same. It is necessary to boost both values up to 4.9 mm/min and 20 m/min, in fiber F, to enhance Rayleigh backscattering up to 26.9 dB, a total of 2 dB related to fiber D, which clearly evinces the change of the kinetics of the system for higher temperatures. Thus, OBR measurements confirm the presence of a slower kinetic at higher drawing temperatures and the possibility of lessening dissolution of Ca-based nanoparticles, as well as tuning the Rayleigh scattering induced at the same time. These findings are a powerful tool to be considered for other Ca-based nanoparticle-doped optical fibers drawn in the range 1870–2065°C, as well as other types of nanoparticle-doped optical fibers for future DOFS based on this technology.

The correlation between Rayleigh backscattering enhancement and the two-way attenuation for the different fibers of this work is plotted in Fig. 6 as well as a comparison with the best reported value, so far, in literature for MgO-based nanoparticle-doped optical fibers for distributed sensing applications, evaluated by OBR [14]. As can be seen, the Ca-based nanoparticle-doped optical fibers display a high performance, in terms of high Rayleigh scattering of light while maintaining relatively low optical losses, with a tuning in the range 24.9–47.4 dB and 0.1–14.6 dB/m, respectively. Therefore, these novel nanoparticle-doped optical fibers allow a broad range

Optical Materials EXPRESS

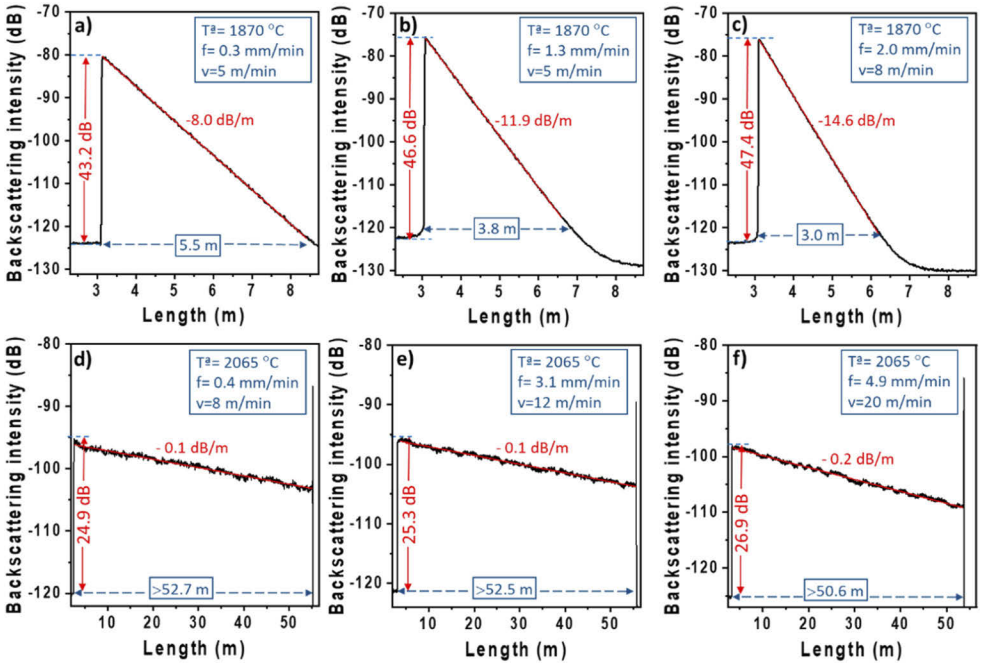

Fig. 5. a-f) Relative backscattering intensity vs fiber length for Ca-based nanoparticles doped fibers A-F, respectively.

of sensing lengths, between 3 m and up to ~250 m. Based on the findings reported in this work and the rest of values includes in Fig. 6 [7], it is expected that for intermediate drawing temperatures, between 1870 °C and 2065 °C, scattering might also be tuned by tailoring the drawing time separately from temperature and thus adjusting it to the targeted application, which locates them in a privilege position for future DOFS. Regarding other nanoparticles considered in literature for this technology, it can be seen that MgO-based nanoparticles grown in situ in silica-based optical fibers also show a good performance, with an enhancement of Rayleigh scattering up to 48.9 dB along with a two-way attenuation of 14.3 dB/m [14]. Compared to other approaches considered in literature for Rayleigh scattering enhanced optical fibers, higher values as well as a better trade-off between scattering enhancement and two-way optical losses are attained. In the case of UV exposure of single mode fibers [21–23], values of 20–37 dB are reported, while for high-numerical aperture fibers, highly Ge-doped and Ge/B-doped, only 10 dB is enhanced [21,22]. In contrast, the inscription of a narrow grating in 25 cm on a single-mode fiber by a femtosecond laser, led to values of 40–45 dB and 2α=15–40 dB/m [24]. However, in these alternatives the fabrication is very slow which hampers the manufacture of large sensing systems. In contrast, the nanoparticle-doped fibers can be manipulated as a standard fiber and then be drawn, spooled, stripped, cleaved and spliced as a standard single mode fiber. Therefore, alkaline earth-based nanoparticles are promising compositions to be considered for distributed sensing applications.

It is worth noticing that these findings show for the first time that Rayleigh scattering enhancement and optical attenuation in nanoparticle-doped silica optical fibers is highly sensitive to several factors during drawing and may be easily tailored by properly adjusting drawing time and drawing temperature, which strongly determine the features of the nanoparticles, both in the plane and along the drawing axis. It is anticipated that these results will pave the way for future works in the field of nanoparticle-doped optical fibers, not only for distributed sensing

Optical Materials EXPRESS

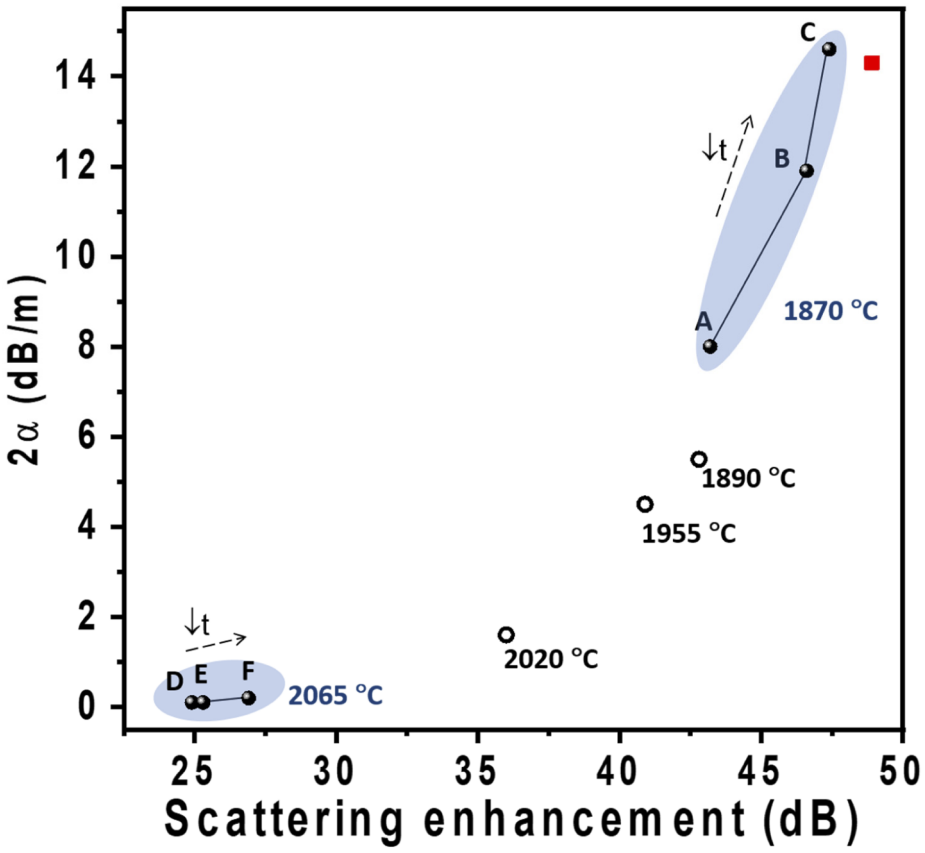

Fig. 6. Scattering enhancement versus two-way attenuation, 2α, extracted from OBR measurements, for the Ca-based nanoparticle-doped silica optical fibers of this work (black solid circles), compared with some of the best reported values in literature for: Ca-based nanoparticles (black empty circles) [7], and MgO-based nanoparticles (red square) [14]. Drawing temperature is indicated in the graph for the Ca-based nanoparticles. The blue patch group the fibers of this work drawn at the same temperature but different drawing time (t). By controlling fiber drawing process, the scattering enhancement and 2α is tuned.

applications, but also for fiber lasers, or broadband sources, among others, in which the tailoring of the nanoparticle characteristics will be closely linked with the required functionality.

3.3. Temperature sensing of Ca-based nanoparticles doped silica optical fibers

With the purpose of testing the temperature sensitivity of these novel Ca-based nanoparticle-doped optical fibers for their use as temperature sensor, an experimental setup as the one depicted in Fig. 7(a) was considered. Optical fibers were immersed in a water bath and heated on a thermal plate in the range 30–120 °C, while spectral shifts in the return loss spectrum were monitored by OBR. The temperature of the plate was monitored by a contact thermocouple and the temperature of the bath by a thermometer to ensure that the temperature distribution was uniform before the measurement was carried out. The reference temperature to calculate the wavelength shifts in the single point depicted in the schema of Fig. 7(a) for every temperature considered was 30 °C. Optical fibers C and D were selected for these experiments, since they present the highest and the lowest Rayleigh scattering values, respectively, with acceptable losses, at the two drawing

Optical Materials EXPRESS

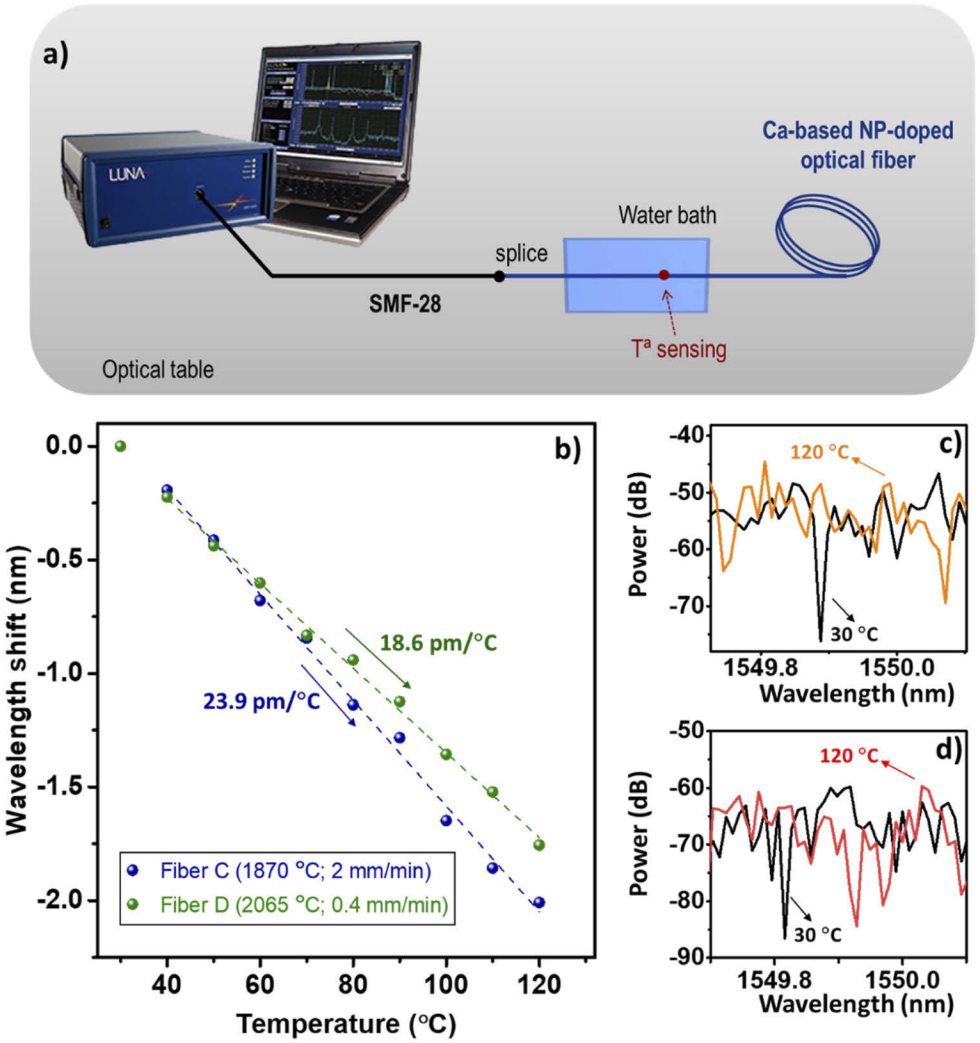

Fig. 7. **a)** Schematic setup used for temperature sensing measurements of Ca-based nanoparticle-doped optical fibers. **b)** Wavelength shift vs Temperature for fiber C and fiber D. The corresponding fiber drawing temperature and preform feed for each fiber is indicated in the legend. Drawing speed for both fibers is 8 m/min. Temperature of the water bath was varied in the range 30–120°C. The spectral signature comparison between 30 °C and 120 °C for **c)** fiber C and **d)** fiber D is shown in a small spectral range to clearly demonstrate that a shift occurs as an effect of heating, avoiding the peak overlapping.

temperatures considered in this work, and therefore allow delimiting the thermal sensitivity at shorter and longer distances of this type of fibers, from 3 m to 250 m, respectively.

From the slope extracted from the linear fitting of the experimental points plotted in Fig. 7, the temperature sensitivity is obtained. It can be concluded that the temperature sensing performance of the Ca-based nanoparticle-doped optical fibers might be effectively tuned, with a sensitivity of 23.9 pm/°C for fiber C and 18.6 pm/°C for fiber D, with an error associated of 0.4 pm/°C and 0.3 pm/°C, respectively. That sensitivity difference is explained in terms of the different nanoparticle features and therefore Rayleigh scattering between these fibers, based on the discussion in section 3.1 and 3.2. It is expected that the sensitivity of the rest of Ca-based nanoparticle-doped

Optical Materials EXPRESS

optical fibers, included in Fig. 5, will be located in the range 18.6–23.9 pm/°C. Comparing these results with the sensitivity reported in literature for MgO-based nanoparticle-doped fibers, 9.1–11.2 pm/°C, standard silica fibers or Bragg gratings, ~10 pm/°C, a considerable improvement of ~1.9–2.4 times is attained [6,14]. The presence of well dispersed Ca-based nanoparticles, with high refractive index, estimated ~1.7 [7], considerably improves the temperature sensing performance of this technology, which along with the possibility of tuning its sensitivity by changing the drawing conditions, which is demonstrated for first time for this novel technology, put this novel type of Ca-based nanoparticle-doped fiber in an advantageous position for sensing applications.

Finally, since some applications need thermal stability at temperatures higher than the typical ones in telecom conditions, ~80°C, as a proof of concept, the fibers are annealed to a temperature considerably higher than the operation temperature in order to guarantee its reliability at that operation temperature [25]. For this purpose, two fiber cuts of fibers C and D are annealed at 520°C for 24 h, and the Rayleigh backscattering spectrum is compared between the annealed fibers and the corresponding as-drawn ones. As it can be observed in Fig. S2 in Supporting information S2, the Rayleigh scattering intensity remains unaltered after the annealing for both fibers and therefore any degradation process occurs in the nanoparticle-doped fibers. It is known that the stability at much lower temperatures is much longer, following an exponential factor [25]. This behavior is contrary to what occurs in UV-processed fibers with fiber Bragg gratings, also considered for sensing applications, in which a thermally induced decay is observed [26]. Thus, Ca-based nanoparticle-doped optical fibers seem to be an interesting candidate for potential high-temperature sensing applications. Moreover, apart from all the above-mentioned advantages, nanoparticle-doped optical fibers are fabricated in standard drawing towers and can be manipulated as standard fiber and thus stripped, cleaved and spliced with losses below 0.1 dB/m, [12] which increases the relevance of this technology for its applications in distributed sensing.

4. Conclusions

In this work, the possibility of tuning Rayleigh scattering and optical losses is demonstrated, and therefore the sensing performance, in Ca-based nanoparticle-doped silica optical fibers through fiber drawing speed, preform feed and drawing temperature. Nanoparticles contained in the preform core are dissolved during fiber drawing process, and a time- and temperature-dependent re-nucleation occurs, which allows the tailoring of factors such as nanoparticle size, number density, and inter-particle distance, as revealed in SEM and FIB-SEM analyses. An early-time kinetics in the re-nucleation process of nanoparticles is inferred at lower drawing temperatures. Consequently, by properly adjusting drawing time at 1870 °C, it is possible to attain a competitive trade-off between Rayleigh backscattering, in the range 43.2–47.4 dB, and two-way optical attenuation, in the range 8.0–14.6 dB/m. Thus, sensing lengths might be adjusted between 3 m and 5.5 m. At higher drawing temperatures the system displays a slower kinetic and these parameters might be adjusted between 24.9–26.9 dB/m and 0.1–0.2 dB/m, respectively. In this case, the fibers are suitable for long-range distributed sensing, from 135 m up to 250 m. Finally, the applicability of Ca-based nanoparticle-doped optical fibers for distributed temperature sensing is demonstrated by OBR. A thermal stability above 500°C and a sensitivity that can be tuned by drawing conditions in the range 18.6–23.9 pm/°C is showed, which implies a sensitivity improvement of ~1.9–2.4 times with respect to a SMF-28.

It is anticipated that these findings might be applied to other nanoparticle-doped optical fibers, allowing the tailoring of their functionalities, which might open a new gate for future works in the field of distributed sensing.

Funding. Canadian Foundation for Innovation; Fonds de recherche du Québec – Nature et technologies (COPL strategic cluster grant); Canada Research Chairs (Advanced photonic Technologies); Canada Excellence Research Chairs,

Optical Materials EXPRESS

Government of Canada (Photonics Innovations); Canada First Research Excellence Fund (Sentinel North Excellence Postdoctoral fellowship).

Acknowledgments. This research was supported by the Sentinel North program of Université Laval, made possible, in part, thanks to funding from the Canada First Research Excellence Fund. The corresponding author, V. Fuertes, holds a Sentinel North Excellence Postdoctoral Fellowship. This research is also supported by the Canadian Excellence Research Chair program (CERCP) in Photonics Innovations, the Canada research chair in Advanced photonic Technologies, the COPL strategic cluster grant by the Fonds de Recherche Québecois sur la Nature et les Technologies (FRQNT), and the Canadian Foundation for Innovation (CFI).

Disclosures. The authors declare no conflicts of interest.

Data availability. Data underlying the results presented in this paper are not publicly available at this time as they also form part of an ongoing study but may be obtained from the authors upon reasonable request.

Supplemental document. See Supplement 1 for supporting content.

References

1. G. Peng, *Handbook of Optical Fibers* (Springer, 2019).
2. T. Giallorenzi, J. A. Bucaro, A. Dandridge, G. H. Sigel, and J. H. Cole, "Optical fiber sensor technology," IEEE Trans. Microwave Theory Techn. **30**(4), 472–511 (1982).
3. W. Blanc and B. Dussardier, "Formation and applications of nanoparticles in silica optical fibers," J. Opt. **45**(3), 247–254 (2016).
4. A. Veber, Z. Lu, M. Vermillac, F. Pigeonneau, W. Blanc, and L. Petit, "Nano-structured optical fibers made of glass-ceramics, and phase separated and metallic particle-containing glasses," Fibers **7**(12), 105 (2019).
5. I. Kasik, P. Peterka, J. Mrazek, and P. Honzatko, "Silica optical fibers doped with nanoparticles for fiber lasers and broadband sources," Curr. Nanosci. **12**(3), 277–290 (2016).
6. A. Beisenova, A. Issatayeva, S. Korganbayev, C. Molardi, W. Blanc, and D. Tosi, "Simultaneous distributed sensing on multiple MgO-doped high scattering fibers by means of scattering-level multiplexing," J. Lightwave Technol. **37**(13), 3413–3421 (2019).
7. V. Fuertes, N. Grégoire, P. Labranche, S. Gagnon, R. Wang, Y. Ledemi, S. Larochelle, and Y. Messaddeq, "Engineering nanoparticle features to tune Rayleigh scattering in nanoparticles- doped optical fibers," Sci. Rep. **11**(1), 1–12 (2021).
8. L. C. Han, S. H. Ding, T. X. Song, L. Huang, X. Y. Zhang, and Z. Xiong, "ZBAS on the structure and dielectric property of $BaAl_2Si_2O_8$," Journal Inorg. Mater. **33**(8), 883–888 (2018).
9. L. Palmieri and L. Schenato, "Distributed temperature sensing based on Rayleigh scattering," Open Opt. J. **7**(1), 104–127 (2013).
10. P. Lu, N. Lalam, M. Badar, B. Liu, B. T. Chorpening, M. P. Buric, and P. R. Ohodnicki, "Distributed optical fiber sensing: review and perspective," Appl. Phys. Rev. **6**(4), 041302 (2019).
11. Z. Ding, C. Wang, K. Liu, J. Jiang, D. Yang, G. Pan, Z. Pu, and T. Liu, "Distributed optical fiber sensors based on optical frequency domain reflectometry: A review," Sensors **18**(21), C1 (2018).
12. D. Tosi, C. Molardi, M. Sypabekova, and W. Blanc, "Enhanced backscattering optical fiber distributed sensors: tutorial and review," IEEE Sensors J. **21**(11), 12667–12678 (2021).
13. W. Blanc, V. Mauroy, and B. Dussardier, "Erbium-doped nanoparticles in silica-based optical fibres," Int. J. Nanotechnol. **9**, 480–487 (2012).
14. D. Tosi, C. Molardi, and W. Blanc, "Rayleigh scattering characterization of a low-loss MgO-based nanoparticle-doped optical fiber for distributed sensing," Opt. Laser Technol. **133**, 106523 (2021).
15. A. Beisenova, A. Issatayeva, I. Iordachita, W. Blanc, C. Molardi, and D. Tosi, "Distributed fiber optics 3D shape sensing by means of high scattering NP-doped fibers simultaneous spatial multiplexing," Opt. Express. **27**(16), 22074 (2019).
16. T. Ayupova, D. Tosi, M. Shaimerdenova, S. Korganbayev, M. Sypabekova, A. Bekmurzayeva, W. Blanc, S. Sales, T. Guo, and C. Molardi, "Fiber optic refractive index distributed multi-sensors by scattering-level multiplexing with MgO nanoparticle-doped fibers," IEEE Sens. J. **20**(5), 2504–2510 (2020).
17. S. Korganbayev, M. Shaimerdenova, T. Ayupova, M. Sypabekova, A. Bekmurzayeva, W. Blanc, C. Molardi, and D. Tosi, "Refractive index sensor by interrogation of etched MgO nanoparticle-doped optical fiber signature," IEEE Photonics Technol. Lett. **31**(15), 1253–1256 (2019).
18. M. Sypabekova, S. Korganbayev, W. Blanc, T. Ayupova, A. Bekmurzayeva, M. Shaimerdenova, K. Dukenbayev, C. Molardi, and D. Tosi, "Fiber optic refractive index sensors through spectral detection of Rayleigh backscattering in a chemically etched MgO-based nanoparticle-doped fiber," Opt. Lett. **43**(24), 5945 (2018).
19. W. Blanc, B. Dussardier, and M. C. Paul, "Er-doped oxide nanoparticles in silica-based optical fibers," Glas. Technol. Eur. J. Glas. Sci. Technol. A. **50**, 79–81 (2009).
20. J. F. White, J. Lee, O. Hessling, and B. Glaser, "Reactions between liquid CaO-SiO_2 Slags and graphite substrates," Metall and Materi Trans B **48**(1), 506–515 (2017).
21. S. Loranger, M. Gagné, V. Lambin-Iezzi, and R. Kashyap, "Rayleigh scatter based order of magnitude increase in distributed temperature and strain sensing by simple UV exposure of optical fibre," Sci. Rep. **5**(1), 11177–7 (2015).

Optical Materials EXPRESS

22. F. Parent, S. Loranger, K. K. Mandal, V. L. Iezzi, J. Lapointe, J.-S. Boisvert, M. D. Baiad, S. Kadoury, and R. Kashyap, "Enhancement of accuracy in shape sensing of surgical needles using optical frequency domain reflectometry in optical fibers," Biomed. Opt. Express **8**(4), 2210 (2017).
23. F. Parent, M. Gérard, F. Monet, S. Loranger, G. Soulez, R. Kashyap, and S. Kadoury, "Intra-arterial image guidance with optical frequency domain reflectometry shape sensing," IEEE Trans. Med. Imaging **38**(2), 482–492 (2019).
24. A. Yan, S. Huang, S. Li, R. Chen, P. Ohodnicki, M. Buric, S. Lee, M. J. Li, and K. P. Chen, "Distributed optical fiber sensors with ultrafast laser enhanced Rayleigh backscattering profiles for real-time monitoring of solid oxide fuel cell operations," Sci. Rep. **7**(1), 1–9 (2017).
25. P.S. Westbrook, K.S. Feder, T. Kremp, E.M. Monberg, H. Wu, B. Zhu, L. Huang, D.A. Simoff, S. Shenk, V.A. Handerek, M. Karimi, A. Nkansah, and A. Yau, "Enhanced optical fiber for distributed acoustic sensing beyond the limits of Rayleigh backscattering," iScience **23**(6), 101137 (2020).
26. T. Erdogan, V. Mizrahi, P. J. Lemaire, and D. Monroe, "Decay of ultraviolet-induced fiber Bragg gratings," J. Appl. Phys. **76**(1), 73–80 (1994).